

# First principles modeling of oxygen adsorption on $\text{LaMnO}_3$ (001) surface

Eugene A. Kotomin<sup>a,b\*</sup>, Yuri A. Mastrikov<sup>a,b</sup>, Eugene Heifets<sup>a</sup> and Joachim Maier<sup>a</sup>

We present and discuss the results of *ab initio* DFT plane-wave  
5 supercell calculations of the atomic and molecular oxygen  
adsorption and diffusion on the  $\text{LaMnO}_3$  (001) surface which  
serves as a model material for a cathode of solid oxide fuel cells.  
The dissociative adsorption of  $\text{O}_2$  molecules from the gas phase is  
energetically favorable on surface Mn ions even on a defect-free  
10 surface. The surface migration energy for adsorbed O ions is  
found to be quite high, 1.6 eV. We predict that the adsorbed O  
atoms could penetrate into electrode first plane when much more  
mobile surface oxygen vacancies (migration energy of 0.69 eV)  
approach the O ions strongly bound to the surface Mn ions. *Ab*  
15 *initio* thermodynamics predicts that at typical SOFC operation  
temperatures ( $\sim 1200$  K) the  $\text{MnO}_2$  (001) surface with adsorbed O  
atoms is the most stable in a very wide range of oxygen gas  
pressures (above  $10^{-2}$  atm).

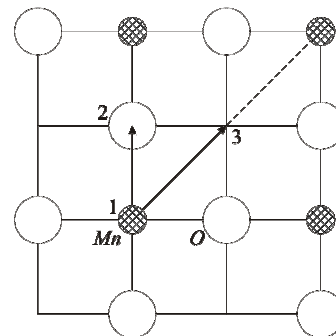
## Introduction

20 Optimization of materials for cathodes of solid oxide fuel cells  
(SOFC) is a scientifically challenging and technologically  
important problem [1]. A necessary prerequisite of systematic  
research is understanding of the mechanism of oxygen reduction  
and in particular, the identification of the rate determining steps  
25 [2]. Despite considerable experimental efforts, many fundamental  
questions remain open. It is in particular the surface diffusion  
step which is poorly understood and which is hard to tackle  
experimentally. At the moment, a most popular SOFC cathode  
materials is Sr-doped  $\text{LaMnO}_3$  (LSM). This material attracted  
30 recently considerable attention also due to its applications in  
spintronics and magnetic cooling [3] which stimulated several  
theoretical studies of magnetic properties of pure LSM surfaces  
[4]. Recently we performed a series of studies of the (100) and  
(110)  $\text{LaMnO}_3$  (LMO) surfaces focused on atomic, electronic and  
35 magnetic structures ([5] and references therein).

However, we are aware only of two literature reports that  
attempted to model at the *ab initio* level an interaction of oxygen  
with LMO and LSM surfaces [6]. In these calculations, a strongly  
polar (110) surface was chosen which consists of alternating  
40 planes  $\text{LaMnO}/\text{O}_2/\text{LaMnO}/\dots$  with opposite charges  $+4e$ ,  $-4e$ ,  
 $+4e\dots$ (per unit cell area). Moreover, the surface unit cell was  
very small and coincides with the bulk unit cell. This is why  
performed modelling of the  $\text{O}_2$  molecule on the  $\text{LaMnO}$ -  
terminated surface in fact has very little in common with a  
45 molecular adsorption but much more with a growth of the proper  
oxygen surface plane above  $\text{LaMnO}$  plane terminating the slab  
used. As is well known [7], stabilization of such polar surfaces  
could be achieved by 50 % reduction of the first plane charge due  
to self-consistent charge redistribution. That is, the  $\text{O}_2$ -terminated  
50 surface is expected to have instead of  $-4e$  a charge of  $-2e$  (per unit  
cell), what was exactly observed by the authors [6] for the  
dissociation products of a  $\text{O}_2$  molecule.

In this Communication, we model O adsorption on a much  
less polar LMO (001) surface consisting of alternating  
55  $\text{MnO}_2/\text{LaO}/\dots$  planes with nominal charges  $\pm 1e$ , and use a large  
surface unit cell corresponding to 12.5 % of surface coverage by  
an adsorbate which corresponds to the SOFC operation  
conditions [1]. Oxygen reduction is complex multi-step process.  
We focus here only on the first stage of the O interaction with  
60 cathode surface which is known to be rate-determining step.

We found optimal sites for atomic and molecular  
adsorption,  $\text{O}_2$  dissociation, and O atom surface diffusion. The  
final step of oxygen interaction with the SOFC cathode is the  
penetration of the adsorbed O atoms into the electrode when they  
encounter surface oxygen vacancies. This is why we calculated  
65 also the migration energy for surface and bulk oxygen vacancies.  
Since the SOFC operates at high temperatures, we complemented  
our DFT calculations by the thermodynamic analysis of the LMO



70 **Fig.1.** Schematic top view of three possible oxygen adsorption sites on  
 $\text{MnO}_2$  (001) surfaces: over Mn (1), O (2) and the hollow position (3). If O  
atom is adsorbed atop surface Mn, the possible saddle points of its  
migration could be positions 2 or 3.

surface stability at such temperatures. Due to electrical neutrality,  
75 motion of charged surface defect is accompanied by the motion  
of surface electronic charge. As the latter does not significantly  
contributes to the activation energy, our results are transformable  
to SOFC fuel cell conditions in which in the steady state  
electrodes are supplied from the outer circuit.

## Method

80 We employed *ab initio* DFT plane-wave-based computer code  
VASP [8] with a plane wave basis set, PAW method to represent  
the atom cores and with the GGA-Perdew-Wang-91 exchange-  
correlation potential, employing the cut-off energy of 400 eV and  
 $2\times 2\times 2$  Monkhorst-Pack k-point mesh in the Brillouin zone [9].  
Preliminary spin polarized calculations of the LMO bulk and the  
85 (001), (110) surfaces are in a good agreement with experiment  
(when available) [5]. In particular, for the experimental  
orthorhombic geometry the energetically most favourable is A-  
type anti-ferromagnetic (AFM) configuration, in agreement with  
experiment whereas the cubic lattice constant (stable above 750  
90 K) exceeds only by 0.5 % the experimental one. The calculated

cohesive energy of 30.7 eV is close to the experimental value (31 eV). Calculations of the surface relaxation and surface energies show a weak dependence on the magnetic configuration [5]. Keeping in mind that relevant effects ( $\sim 0.1$  eV [5,6]) are much smaller than the adsorption and migration energies under study (several eV) and that under operation SOFC conditions LMO is paramagnetic ( $T_N=140$  K), we performed all calculations for the ferromagnetic (FM) state with collinear spins. Moreover, the FM slab has the lowest energy. Neglect of spin polarisation results in considerably errors in material properties. We found in particular that 7- and 8- plane slabs are thick enough and show main property convergence.

For modelling oxygen adsorption based on our studies of pure surfaces [9], we used here a 7-plane slab terminated on both sides with  $\text{MnO}_2$  plane covered by the adsorbate. Use of such symmetrical slab permits to avoid a problem of the surface dipole moment [7]. The periodically repeated slabs were separated by a vacuum gap of 15.8 Å (which corresponds to the thickness of 8-plane slab). The chosen surface unit cell was the extended  $2\sqrt{2} \times 2\sqrt{2}$  primitive unit cell, i.e. the surface coverage was 1/8 (12.5%).

Since our calculations correspond to 0 K, we used the relevant low-temperature *orthorhombic* unit cell with on-plane lattice constants  $a=5.56$  Å,  $b=5.61$  Å optimized for the bulk. All atomic coordinates were allowed to relax. Based on our experience for O adsorption on the  $\text{SrTiO}_3$  (001) surface [10], we studied oxygen adsorption over surface Mn, O ions and the hollow position (Fig.1). The topological (Bader) effective atomic charges were calculated according to method described in Ref. [11]. The oxygen atom adsorption energies  $E_{\text{ads}}^{(\text{at})}$  were calculated with respect to free oxygen atoms:

$$E_{\text{ads}}^{(\text{at})}(\text{O}) = -\frac{1}{2} [E_{\text{slab}}^{(\text{ads})}(\text{O}) - E_{\text{slab}} - 2E^{(\text{O})}], \quad (1)$$

and with respect to free oxygen molecule:

$$E_{\text{ads}}^{(\text{m})}(\text{O}) = -\frac{1}{2} [E_{\text{slab}}^{(\text{ads})}(\text{O}) - E_{\text{slab}} - E^{(\text{O}_2)}], \quad (2)$$

where  $E_{\text{slab}}^{(\text{ads})}$  is the total energy of a fully relaxed slab with two-sided adsorbate (O or  $\text{O}_2$ ),  $E_{\text{slab}}$  is the same for a pure slab,  $E^{(\text{O})}$  is the energy of isolated oxygen atom in the ground triplet state, and  $E^{(\text{O}_2)}$  is the total energy of isolated oxygen molecule in the triplet state. The prefactors  $\frac{1}{2}$  before brackets and 2 before  $E^{(\text{O})}$  appear since the interface is modeled by a substrate slab with two equivalent surfaces and both  $\text{O}_{\text{ads}}$  atoms and  $(\text{O}_2)_{\text{ads}}$  molecule symmetrically positioned on both sides of the slab. The molecular adsorption energy was calculated in a similar way. The difference of  $E_{\text{ads}}^{(\text{at})}(\text{O})$  and  $E_{\text{ads}}^{(\text{m})}(\text{O})$  equals to the  $\text{O}_2$  molecule binding energy.

## Results and Discussion

### Adsorption positions and energies

Table 1 shows a strong preference for O atom adsorption over the surface Mn ion, unlike the bridge position between Ti and O ions found for the isostructural  $\text{SrTiO}_3$  [10]. The difference is in line with the oxidizability of  $\text{Mn}^{3+}$  (compared to  $\text{Ti}^{4+}$ ). Note that the top of the valence band in  $\text{LaMnO}_3$  is largely due to Mn orbitals whereas the O orbitals generate the valence band top in  $\text{SrTiO}_3$ . The electron charge of 0.62 e is transferred to the adsorbed O atom from nearest surface ions (0.18 e from

nearest Mn, 0.16 e from four nearest O ions and the rest 0.28 e from next-nearest ions).

The analysis of the electron density redistribution confirms that the O adsorption induces a quite local perturbation.

In the total density map one can see very well the “wavy” atomic structure of the orthorhombic slab. As a result of O adsorption, the spin momentum of Mn ion is strongly reduced.

The test calculations performed for the high-temperature *cubic* phase ( $T > 750$  K) give qualitatively similar results. In particular, the adsorption energy atop the Mn ion is 4.14 eV,  $\sim 3\%$  larger than in the orthorhombic phase.

In order to check how use of the nonstoichiometric slab affects the adsorption energy, we repeated calculations for the stoichiometric cubic 8-plane slab. The O adsorption energy atop Mn ion increased by 0.25 eV, or 6%. The adsorbed O charge practically does not change (-0.64 e and -0.61 e, respectively) whereas the Mn ion charges exceed those on the perfect surface by 0.21 e and 0.1 e for 7- and 8-plane slabs, respectively. The atomic charges on 7-plane cubic and orthorhombic surfaces are very close.

The adsorption position near the surface O ion is practically identical to the *bridge position* found to be energetically most favourable for the  $\text{SrTiO}_3$  (001) surface [10]. For  $\text{LaMnO}_3$ , this configuration turns out to be energetically less favourable, and the position above the hollow point the most

**Table 1.** Calculated adsorption properties for O atoms on  $\text{MnO}_2$  (001) orthorhombic surface. Energies in eV, distances from nearest ions, in Å, spins in  $\mu_B$ , S, T stand for singlet and triplet. The effective atomic charges on a pure surface: 1.67 e (Mn), -1.17 e (O). 2x, 4x indicate a number of equivalent atoms.

Site	$E_{\text{ads}}^{(\text{at})}(\text{O})$	$E_{\text{ads}}^{(\text{m})}(\text{O})$	Distance from $\text{O}_{\text{ads}}$		Charges			Spin	
			$\text{O}_s$	$\text{Mn}_s$	$\text{O}_s$	$\text{Mn}_s$	$\text{O}_{\text{ads}}$	Mn	O
Mn	4.02	1.07	2.55(4x)	1.63	-1.13	1.85	-0.62	2.20	S
O	2.41	-0.54	1.50 <sup>a)</sup>	1.87	-0.71	1.65	-0.48	3.61	S
Hollow	0.59	-2.36	3.28(2x)	---	-1.16	----	-0.32	---	T
			3.18(2x)	---	(4x)				

<sup>a)</sup>The O-O dumbbell has an angle of  $50^\circ$  with the normal to the surface

unfavourable. In these two cases the adsorbed O atom receives 0.3-0.5 e from the nearest surface ions. Keeping in mind that the effective charges in LMO bulk and on the surface are considerably reduced due to the covalent component in the Mn-O chemical bonding as compared to the nominal charges ([5] and heading in Table 1), the configuration above the O ion could be treated as formation of a kind of  $\text{O}_2^{(2-)}$  peroxo-molecule [6] tilted by  $50^\circ$  towards nearest Mn ion.

The calculated adsorption energies with respect to an O atom in a free molecule,  $E_{\text{ads}}^{\text{m}}$ , Eq. (2), are collected in Table 1. The positive value is obtained only for O atom atop the Mn ion, where the energy gain due to adsorption of two O atoms is larger than the molecule dissociation energy. (Despite the fact that our calculations overestimate the dissociation energy of a  $\text{O}_2$  molecule -- 5.9 eV vs experimental 5.12 eV [12] -- this does not affect our conclusion.)

## Oxygen migration

The most stable position of the adsorbed O atom is atop of the surface Mn ion. Based on our results, the adsorbed O atom migration could occur with the barrier located nearby the O surface ion and with the activation energy exceeding 1.6 eV. Since the adsorbed oxygen atoms turned out to be strongly bound to the surface Mn ions and thus are quite immobile, penetration of these O atoms into the first plane of fuel cell cathode can occur predominantly upon their encounter with the mobile surface oxygen vacancies. Following our SrTiO<sub>3</sub> study [14], we calculated the equilibrium and saddle points for oxygen vacancies in the bulk and on the MnO<sub>2</sub> terminated surface (see also [13]). In the latter case, two pairs of nearest Mn and La ions are strongly displaced from the vacancy (ca. 0.2 Å) whereas the two O ions towards the vacancy (0.32 Å). The negative charge of the missing O ions is spread over nearest ions, mostly Mn. The calculated vacancy migration energy is 0.67 eV, smaller than that calculated for the bulk (0.95 eV). The latter value is typical for ABO<sub>3</sub> perovskites (see e.g. experimental data [14]) whereas the reduced energy on the surface also is in line with the trend in our calculations for vacancies in SrTiO<sub>3</sub> [15]. More detailed results will be published elsewhere. The key point here is that the vacancy mobility is much higher than that of the adsorbed O atoms and thus vacancy migration along cathode surface enables fast O transport to the electrode.

## Molecular adsorption

Along with the O atom adsorption, we calculated also the O<sub>2</sub> molecular adsorption over the energetically most favorable position atop the Mn ion in the two configurations: perpendicular and parallel to the surface (called hereafter *tilted* and *horizontal* in Table 2). The molecule binding energy is larger for the tilted adsorption (Table 2). The total charge of the adsorbed molecule is

**Table 2.** Calculated adsorption properties for O<sub>2</sub> molecules on MnO<sub>2</sub> surface. Notations as in Table 1.

Oriented	E <sub>ads</sub> <sup>(m)</sup> (O <sub>2</sub> )	Distances		Charges <sup>b)</sup>			Spin
		O-O bond	O-Mn <sub>s</sub>	O(1)	O(2)	Mn <sub>s</sub>	
Tilted	1.13	1.36	1.86 <sup>a)</sup>	-0.29 <sup>a)</sup>	-0.13	1.78	3.12 T
horizontal	0.89	1.42	1.85	-0.30	-0.30	1.77	3.05 D
			1.90				

a)For O atom nearest to the surface , b) Atoms in O<sub>2</sub> molecule c)3.80 μ<sub>B</sub> on a pure surface

-0.42 e and the bond length 1.36 Å. (The bond length 1.3 Å of a free O<sub>2</sub> molecule calculated for the cutoff energy and other parameters used in this study are slightly larger than experimental value of 1.21 Å [12]). The adsorbed molecule could be considered as a kind of the superoxo-radical O<sub>2</sub><sup>-</sup>[6].

In the horizontal configuration the total charge of the molecule is larger, -0.6 e, the bond length increases up to 1.42 Å and it is closer to the peroxo-radical O<sub>2</sub><sup>2-</sup>. In both cases we observe chemisorption (unlike a weak physical adsorption of O<sub>2</sub> on SrTiO<sub>3</sub> (001) surface). A comparison of atomic and molecular adsorption energies (Tables 1 and 2), indicates that 2E<sub>ads</sub><sup>(m)</sup>(O)<sup>></sup>E<sub>ads</sub><sup>(m)</sup>(O<sub>2</sub>) for the most favorable adsorption site atop

the Mn ion. This means that the *dissociative* molecular adsorption is favorable even on the defectless surface – in contrast to SrTiO<sub>3</sub> [10].

## Surface stability under SOFC operation conditions

In order to analyze the relative stability of different LaMnO<sub>3</sub> surfaces under realistic operation conditions of the fuel cell, we performed the *ab initio* thermodynamic treatment, similar to that applied earlier to BaZrO<sub>3</sub> [16] and SrTiO<sub>3</sub> [17] surfaces. This method was developed following a general *ab initio* thermodynamic approach ([18-23] and references therein). The most stable surface at any considered oxygen and manganese chemical potentials has the lowest surface Gibbs free energy.

(Note that we do not consider vibrational entropy changes which are supposed to be small [18].) We considered LaO- and MnO<sub>2</sub>-terminated (001) surfaces built of *cubic* (high temperature) unit cells; LaMnO-, O<sub>2</sub>-, and O-terminated (110) surfaces, and, finally, MnO<sub>2</sub>-terminated (001) surface with adsorbed O atom (hereafter MnO<sub>2</sub>+O- terminated surface). Since we assume the equilibrium of the surface with the bulk where the chemical potentials of three crystal constituents (La, Mn, and O) are interrelated by the condition μ(LaMnO<sub>3</sub>)=μ(La)+μ(Mn)+3μ(O), only chemical potentials of two of these components are independent variables. Because oxygen atoms are in equilibrium in the surface and in the O<sub>2</sub> gas above the cathode surface and we have to account for a strong dependence of O chemical potential on the O<sub>2</sub> gas partial pressure and temperature, it is suitable to

**Table 3** Calculated formation enthalpies ΔE<sub>f</sub> (eV) for bulk oxides and LaMnO<sub>3</sub> perovskite. The second column contains experimental formation enthalpies for the oxides and LaMnO<sub>3</sub> [24] at T<sub>0</sub>=298.15 K, p<sub>0</sub>=1 atm. The last column provides a correcting shift of the experimental Gibbs free energies for O<sub>2</sub> gas calculated using different oxides (Ref. [16,17]).

Crystal	Calc. E <sub>f</sub> , eV	Expt ΔH <sub>f</sub> , eV
La <sub>2</sub> O <sub>3</sub>	-18.86	-18.60
Mn <sub>2</sub> O <sub>3</sub>	-11.57	-9.92
MnO	-4.19	-3.99
MnO <sub>2</sub>	-7.03	-5.39
Mn <sub>3</sub> O <sub>4</sub>	-16.70	-14.37
LaMnO <sub>3</sub>	-15.66	-14.77
LaMnO <sub>3</sub> (from La <sub>2</sub> O <sub>3</sub> and Mn <sub>2</sub> O <sub>3</sub> oxides)	-0.498	-0.514

choose the O chemical potential as one of independent variables in the surface Gibbs free energy whereas the Mn chemical potential can be taken as another independent variable. Following [16,17], we calculate these quantities with respect to the energy per atom in Mn metal (Δμ(Mn)) and O atom in a free O<sub>2</sub> molecule (Δμ(O)).

We plotted the phase diagram on the l.h.s. of Fig. 2 which shows stability regions of different surfaces. The colour area here is limited at the bottom by the line, where the chemical potential of La atoms in LMO becomes larger than in a metal, what corresponds to a La precipitation. On other sides, the coloured area is limited by lines, where the lowest surface Gibbs free energies become negative and crystal spontaneously disintegrates. Only four different surfaces from six considered could be stable: LaO-terminated (001) surface, MnO<sub>2</sub>+O-

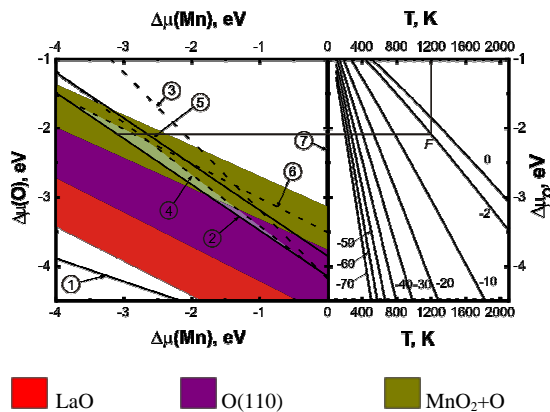


**Fig. 2** (Color). The phase diagram: the regions of stability of  $\text{LaMnO}_3$  surfaces with different terminations as functions of chemical potential variation for Mn and O atoms. Comparison includes  $\text{LaMnO}_3$ -,  $\text{O}_2$ -, and O-terminated (011) surfaces,  $\text{LaO}$ - and  $\text{MnO}_2$ - terminated (001) surfaces, and  $\text{MnO}_2$ -terminated (001) surface with adsorbed O atom. The numbers in circles points to the lines, where metals or their oxides begin to precipitate: (1) metal La, (2)  $\text{La}_2\text{O}_3$ , (3)  $\text{MnO}_2$ , (4)  $\text{Mn}_3\text{O}_4$ , (5)  $\text{Mn}_2\text{O}_3$ , (6) MnO, and (7) metal Mn. The right side of the figures contains a family of  $\Delta\mu_{\text{O}}$  as functions of the temperature at different oxygen gas pressures. The labels  $m$  on the oxygen lines indicate the gas pressure:  $10^{-m}$  atm.

terminated (001) surface, O- and  $\text{O}_2$ - terminated (110) surfaces (the latter one is not seen in Fig. 4 within shown range of chemical potentials)

To determine the boundaries of the region, where precipitation of La- and Mn oxides does not occur, we computed the *formation energies* (enthalpies) for related metal oxides. Results for the oxide formation energies are provided in Table 3, where calculations are also compared with experimental formation enthalpies. Our computations slightly overestimate the formation energies, what is commonly observed for the DFT with GGA functionals. Still, when we considered formation of  $\text{LaMnO}_3$  perovskite from the oxides with the same oxidation states as in the perovskites, the obtained value matches very well to that derived from experimental data.

The boundaries of the region, where  $\text{LaMnO}_3$  crystal is stable with respect to decomposition into metals and their oxides, are represented in Fig.2 by lines 1 to 7. Pure  $\text{LaMnO}_3$  surfaces could exist only between these lines [16,17]. The stability region is limited by line 2 (precipitation of  $\text{La}_2\text{O}_3$ ) on the bottom and by lines 4 and 6 (precipitation of  $\text{Mn}_3\text{O}_4$  and MnO, respectively) on the top. Because of the DFT shortcoming in calculations of the relative energies for materials with different degree of metal oxidation, one has to treat the obtained data with some caution. Therefore, we highlighted lines of precipitation for 3-valent metal oxides  $\text{La}_2\text{O}_3$  and  $\text{Mn}_2\text{O}_3$  (solid lines 2 and 5), where the oxidation state is the same as in  $\text{LaMnO}_3$ . From all considered surfaces, only *two* turn out to be stable (within the region of  $\text{LaMnO}_3$  crystal stability): (i)  $\text{MnO}_2$ -terminated (001) surface with adsorbed O atoms ( $\text{MnO}_2+\text{O}$  surface) at high O chemical potentials (O-rich limit) and low Mn chemical potential (Mn-poor limit) and (ii) O-terminated (110) surface at low O chemical potentials (O-poor limit) and high Mn chemical potential (Mn-reach limit). This result remains valid, whatever we include into consideration only precipitation of 3-valent La and Mn oxides or

also account for possible precipitation of all other manganese oxides.

On the r.h.s. of Fig. 2 we plotted the chemical potentials of the O atom derived from the experimental data (Ref. [24]). This window shows the dependence of the O chemical potential on temperature and  $\text{O}_2$  partial pressure. Correct matching of the experimental curves with the computed stability diagram requires a correcting shift of the O atom chemical potential as explained in detail in ref. [16,17]. We calculated the shift employing the same set of oxides used in this work and thus obtained the average shift of -0.77 eV value used in Fig. 2.

The combination of our surface stability diagram with the oxygen chemical potential as a function of the temperature and  $\text{O}_2$  partial pressure allows a detailed analysis of the trends under variable environmental conditions. Let us consider a situation typical for the fuel cell operation:  $T \approx 1200$  K and oxygen partial pressure ranging between  $p_{\text{O}_2} = 0.2$  and 0.01 atm (point F in Fig. 2). Our stability diagram demonstrates clearly that only the  $\text{MnO}_2$ -terminated (001) cubic surface with adsorbed O atoms is stable under the operational conditions (large O chemical potential, relatively high O pressure). The alternative (110) surface becomes dominant only at low O chemical potentials and thus very low oxygen pressures,  $p_{\text{O}_2} \leq 10^{-10}$  atm.

## Conclusions

Under operational conditions of a fuel cell cathode, the cubic  $\text{MnO}_2$  surface with adsorbed O atoms (with a considered coverage of 12 %) is the most stable (in particular, more stable than (110) surfaces).

We have demonstrated that  $\text{LaMnO}_3$  (001) surface could be catalytically more active than isostructural  $\text{SrTiO}_3$  since it permits dissociative  $\text{O}_2$  desorption on surface Mn ions without assistance of surface defects. The penetration of adsorbed O atoms into the first plane of cathode occurs very likely when it meets highly mobile surface O vacancies. The vacancy migration energy (0.67 eV) along the surface is smaller than in the bulk (0.95 eV) and enables fast surface diffusion of oxygen in the first cathode layer (rather than in the adsorbed state with the activation energy exceeding 1.6 eV). We do not expect entropy effects to be large enough as to favour the diffusion in the adsorbed state over surface diffusion in the first layer; however it may seriously favour bulk diffusion at very high temperatures. Quantum MD simulations would be of great interest to clarify this point.

## Acknowledgments

Authors are greatly indebted to R. Merkle, D. Fuks, M. Liu, N. Kovaleva, J. Fleig, Yu. Zhukovskii and H.-U. Haberman for many stimulating discussions.

## Notes and references

- <sup>a</sup> Max Planck Institute for Solid State Research, Heisenbergstr., 1, D-70569, Stuttgart, Germany. Fax: 49 711689 1722; Tel: 49 711689 1721, E-mail: sofia.weiglein@fkf.mpg.de
- <sup>b</sup> Institute for Solid State Physics, University of Latvia, Kengaraga str. 8, Riga LV-1063, Latvia. Fax: 371 7132 778; Tel: 371 7187 816; E-mail: kotomin@fkf.mpg.de

1. J. Fleig, K.D. Kreuer, and J. Maier, In: *Handbook of Advanced Ceramics*, Singapore, Elsevier, 2003, p. 57; J. Fleig, R. Merkle, and J. Maier, *Phys Chem Chem Phys*, 2007, **9**, 2713.
2. R. Merkle and J. Maier, *Topics in Catalysis*, 2006, **38**, 141.
- 5 3. M. Bowen, M. Bibes, A. Barthélémy, J.-P. Contour, A. Anane, Y. Lemaître, and A. Fert, *Appl. Phys. Lett.*, 2003, **82**, 233.
4. G. Banach and W.M. Temmerman, *Phys. Rev. B*, 2004, **69**, 054427; H. Zenia, G.A. Gehring, G. Banach and W. M. Temmerman, *Phys. Rev. B*, 2005, **71**, 024416.
- 10 5. R.A. Evarestov, E.A. Kotomin, Yu.A. Mastrikov, D. Gryaznov, E. Heifets, and J. Maier, *Phys. Rev. B*, 2005, **72**, 214411, E.A. Kotomin, R.A. Evarestov, Yu.A. Mastrikov and J. Maier *Phys. Chem. Chem. Phys.*, 2005, **7**, 2346 - 2350
- 15 6. Y. Choi, D.S. Mebane, M.C. Lin, and M. Liu, *Chem. Mater.* 2007, **19**, 1690; Y. Choi, M.C. Lin, M. Liu *Angewandte Chemie*, 2007, **119**, 7352.
7. C. Noguera, *Physics and Chemistry of Oxide Surfaces*, Cambridge Univ. Press, NY., 1996.
- 20 8. G. Kresse and J. Furthmüller, *VASP the Guide*, University of Vienna, Austria, 2003.
9. H.J. Monkhorst and J.D. Pack, *Phys. Rev. B*, 1976 **13**, 5188.
10. S. Piskunov, E.A. Kotomin, Yu.F. Zhukovskii, E. Heifets, and D.E. Ellis, *Mater. Res. Symp. Proc.*, 2005, **894**, LL05-05.1.
11. G. Henkelman, A. Arnaldsson and H. Jónsson, *Comp. Mater. Sci.*, 2006, **36**, 354.
- 25 12. CRC Handbook of Chemistry and Physics, ed. D.R. Lide, CRC Press, Boca Raton, FL, 1993.
13. Yu. Zhukovskii, E.A. Kotomin, R.A. Evarestov, and D.E. Ellis, *Int. J. Quant. Chem*, 2007, **107**, 2956 (review article).
- 30 14. Denk, W. Munch and J. Maier, *J. Am. Cer. Soc.*, 1995, **78**, 3265.
15. J. Carrasco, F. Illas, N. Lopez, E. A. Kotomin, Yu. F. Zhukovskii, R. A. Evarestov, Yu. A. Mastrikov, S. Piskunov and J. Maier, *Phys. Rev. B*, 2006, **73**, 064106.
- 35 16. E. Heifets, J. Ho, B. Merinov, *Phys. Rev. B*, 2007, **75**, 155431.
17. E. Heifets, S. Piskunov, E.A. Kotomin, Yu. F. Zhukovskii and D. E. Ellis, *Phys. Rev. B*, 2007, **75**, 115417.
18. K. Reuter, M. Scheffler, *Phys. Rev. B*, 2001, **65**, 035406.
19. K. Johnston, M. R. Castell, A. T. Paxton, and M. W. Finnis, *Phys. Rev. B*, 2004, **70**, 085415.
- 40 20. J. Padilla and D. Vanderbilt, *Surf. Sci.*, 1998, **418**, 64.
21. F. Bottin, F. Finocchi, and C. Noguera, *Phys. Rev. B*, 2003, **68**, 035418.
22. J.W. Cahn, In: *Interfacial Segregation*, W.C. Johnson and J.M. Blacely (eds.) (Am.Soc. for Metals, Metals Park, Ohio, 1977), p.3-23.
- 45 23. I. Batyrev, A. Alavi and M.W. Finnis, *Farad. Disc.*, 1999, **114**, 33.
24. M.W. Chase, *NIST-JANAF Thermochemical Tables* (Am. Chem. Soc., Washington, DC, 1998).
- 50

55